Thermal Denaturation of Beta-Lactoglobulin and Stabilization Mechanism by Trehalose Analyzed from Raman Spectroscopy Investigations

Jeong-Ah Seo,[†,‡] Alain Hédoux,[*,†] Yannick Guinet,[†] Laurent Paccou,[†] Frédéric Affouard,[†] Adrien Lerbret,[†] and Marc Descamps[†]

Unité Matériaux Et Transformations, UMR CNRS 8207, Université de Lille 1, 59655 Villeneuve d Ascq Cédex, France, and School of Engineering and Applied Sciences, Harvard University, Cambridge, Massachusetts 02138

Received: January 21, 2010; Revised Manuscript Received: April 8, 2010

The thermal denaturation process of beta-lactoglobulin has been analyzed in the 20−100 °C temperature range by Raman spectroscopy experiments simultaneously performed in the region of amide modes (800−1800 cm^{-1}) and in the low-frequency range (10−350 cm^{-1}). The analysis of amide modes reveals a two-step thermal denaturation process in the investigated temperature range. The first step corresponds to the dissociation of dimers associated with an increase of flexibility of the tertiary structure. In the second step, large conformational changes are detected in the secondary structure and described as a loss of α-helix structures and a concomitant formation of β-sheets. Raman investigations in the low-frequency range provide important information on the origin of the denaturation process through the analysis of the solvent dynamics and its coupling with that of the protein. The softening of the tetrahedral structure of water induces the dissociation of dimers and makes the tertiary structure softer, leading to the water penetration in the protein interior. The methodology based on Raman investigations of amide modes and in the low-frequency region was used to analyze the mechanism of beta-lactoglobulin thermostabilization by trehalose. The main effect of trehalose is determined to be related to its capabilities to distort the tetrahedral organization of water molecules.

I. Introduction

The exceptional properties of trehalose to stabilize biomolecular systems are now well recognized,[1,2] and widely used to protect proteins from the stresses that arise during purification or freeze-drying procedures induced by freezing or dehydration.[3−5] The numerous hypotheses[6−12] suggested for understanding the bioprotection mechanisms are generally suitable for narrow temperature and hydration ranges, that prevent a complete description of these mechanisms. As a consequence, the choice of the solutes used in freeze-drying processes and the development of stable formulations are still largely empirical.

Recent investigations carried out on lysozyme[13−15] and bovine serum albumin[16] thermal denaturations have pointed out a common mechanism of bioprotection by disaccharides. A detailed analysis on lysozyme[14] has clearly shown that trehalose was the most efficient bioprotectant to preserve the native conformation of the protein against high temperatures. The combination of Raman investigations[14,15] and molecular dynamics simulations[17] has shown that the mechanism of lysozyme thermostabilization by disaccharides was the result of two complementary effects. First, sugars have a destructuring effect on the tetrabonded H-bond network of water, in agreement with analyses performed on water/sugar solutions.[9,17,18] As a consequence, O−H intermolecular interactions in the H-bond network of water are strengthened, leading to the stabilization of the tertiary structure of lysozyme. Second, sugars are excluded from the protein surface, and preserve the hydration shell of the protein, in line with the preferential hydration hypothesis.[12] However, experimental evidence of protein thermostabilization is correlated to the protein denaturation process and then highly dependent on the protein structure. The results obtained on lysozyme were confirmed by a similar analysis on bovine serum albumin,[16] which has similar structural characteristics. To get a general description of the bioprotection mechanism in the high temperature range, the influence of bioprotectants on the thermal denaturation of different proteins must be investigated.

The secondary structure of bovine serum albumin[19,20] (BSA) is characterized by a high α-helix content (∼51%) and quasi none β structure, while lysozyme[19,20] is composed of α-helices (41%) and β-sheets (21%). In contrast, β-lactoglobulin (BLG) is mainly composed of β-sheets (54%) and α-helices (17%).[21] At native pH, this protein of 162 residues is found in a dimeric conformation, while, at acidic pH, it dissociates into monomers, recognized as more stable than the native state.[22,23] BLG is a globular protein widely analyzed for investigation of heat-induced aggregation.[24−26] The thermal denaturation process of BLG was described as a multistep mechanism and highly dependent on the protein concentration and pH.[27−29] At neutral and alkaline pH values and physiological concentrations (<5 wt %), the dissociation of the dimer is coupled with a conformational transition to an R-type state, around 40−55 °C. The native (N) to the R-state transition was associated with a single anomalous carboxyl group which appears to be buried in the hydrophobic interior of the protein in conformation N, and becomes exposed to the surface in conformation R.[30] The folding of the main polypeptide chains is not altered passing through this transition. A progressive loss of β-sheet structure was observed with increasing temperature, while an abrupt loss of the helical conformation was detected near 65 °C.[27] At high protein concentrations for acidic and alkaline pH, calorimetric measurements led to the interpretation of the BLG thermal

* Corresponding author. E-mail: alain.hedoux@univ-lille1.fr. Phone: +33 320434677. Fax: +33 320436857.
† Université de Lille 1.
‡ Harvard University.

10.1021/jp1006022
Published on Web 04/22/2010

denaturation as a two-step process, in which the monomeric intermediate and the denatured state would occur slightly below 70 °C and around 140 °C,[28] respectively. Raman investigations[26] carried out on BLG solutions (15 wt % in D_2O, pD 6.8) have revealed a different transformation of the secondary structure after heating between 70 and 90 °C, described as an increase of β-sheet structure with a simultaneous decrease of turn structure.

The main objective of this paper is to determine the influence of bioprotectant on the stability of native BLG and to give additional information to previous analyses for understanding the physical mechanism of bioprotection. Taking into account the dependence of the denaturation process on pH and concentration, and the controversial descriptions of the denaturation process, a careful analysis of thermal denaturation of BLG is needed prior to the study of the stabilization induced by bioprotectants.

Thermal denaturation of BLG is analyzed by Raman spectroscopy investigations simultaneously carried out in the low-frequency range (10−350 cm^{-1}) and in the amide band region (800−1800 cm^{-1}), which is widely analyzed to determine the secondary structure of proteins, and the structural changes induced by protein denaturation. BLG was systematically dissolved in D_2O, since Raman spectroscopy gives the opportunity to analyze isotopic exchanges which could reflect structural changes in the tertiary or quaternary structure, with intact secondary structure.[15,16] In this way, the transformation of the tertiary structure of lysozyme during thermal denaturation[13] was detected by enhanced isotopic exchanges induced by the penetration of the solvent into a more flexible tertiary structure.

The low-frequency Raman spectrum (LFRS) mainly[13] reflects the protein dynamics, and gives information on the H-bond network of water.[13] This analysis is then crucial to understand the origin of structural changes in the protein.

II. Materials and Methods

Beta-lactoglobulin (BLG, 18.4 kDa), bovine serum albumin (BSA, 66 kDa), and alpha-chymotrypsin (CHYM, 22.3 kDa) were purchased from Sigma as lyophilized powder (purity minimum 90% for BLG, 85% for CHYM, and 98% for BSA). BLG solutions were first prepared in the absence of trehalose (T) by dissolving BLG at various concentrations (5, 10, and 15 wt %) in D_2O (W_d). High-purity anhydrous trehalose was supplied from Fluka and Sigma. For ternary mixtures (BLG/W_d/T), trehalose water mixtures (W_d/T) were prepared at the desired concentrations (10, 20, 30, and 40 wt % trehalose) and thereafter the protein was added. The protein containing mixtures were agitated in an Eppendorf agitator at about 298 K with about 1000 turns/min. The mixtures were loaded in spherical glass cells and hermetically sealed. Measurements were carried out in the 20−100 °C temperature range on samples at pD 6.9.

Raman spectroscopy was performed using an XY Dilor spectrometer with a 514.5 nm Ar−Kr laser and 20 mW of incident power. Spectra were recorded in the 10−350 cm^{-1} range and in the 800−1800 cm^{-1} range (amide band region) by measuring in backscattering geometry. The spectrometer is composed of a double monochromator comprising four mirrors characterized by a focal length of 800 mm and a spectrograph. The entrance and exit slits are opened and kept at 300 μm, determining the incident radiation at a resolution of nearly 2 cm^{-1} in the low-frequency range. It is the monochromator which prohibits the exciting line from entering the spectrograph field. The well-adapted positioning of the monochromator with respect to the spectrograph and the choice of experimental conditions (incident radiation, slit width) allow a rejection of exciting light down to 10 cm^{-1}. The spectrometer is equipped with a liquid nitrogen cooled charge coupled device detector. The high sensitivity of the detector allows us to record the low-frequency spectra between 10 and 350 cm^{-1} in 5 min and the 800−1800 cm^{-1} region in 15 min. A fluorescence contribution to the spectra appeared systematically in the background signal. Its magnitude was approximated by a second order polynomial using a fitting procedure, and then subtracted from the spectra.

Raman investigations were performed between 20 and 100 °C using an Oxford nitrogen-flux device that keeps temperature fluctuations within 0.1 °C.

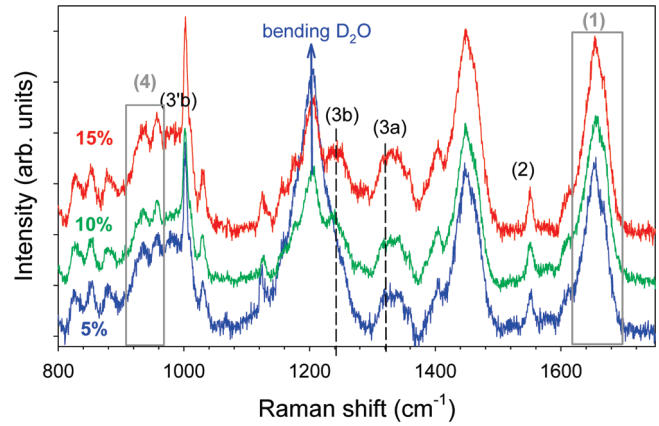

Figure 1. Raman spectrum of BLG dissolved in D_2O for 5, 10, and 15% (wt) protein concentrations in the 800−1800 cm^{-1} region.

III. Results

III.1. Analysis of BLG Thermal Denaturation. BLG solutions (5, 10, 15 wt % in D_2O) were analyzed at room temperature in the low-frequency range (10−350 cm^{-1}) and in the amide band region (800−1800 cm^{-1}).

III.1.a. Investigations of the Amide Modes in the 800−1800 cm^{-1} Region. At room temperature, the Raman spectra of aqueous BLG solutions [5, 10, 15% (wt) in D_2O, pD 6.9] in the 800−1800 cm^{-1} region are plotted in Figure 1, for the assignment of Raman bands. The spectra were baselined and normalized to the phenylalanine band located at 1004 cm^{-1} which was observed to be temperature independent.

The Raman spectrum of BLG solution (5 wt %) is dominated by a band located around 1200 cm^{-1}. The intensity of this band decreases as a function of the protein concentration. It is assigned to the bending vibration in D_2O.

For protein concentrations higher than 5%, the most intense band of the spectrum, located around 1650 cm^{-1}, is the amide I band (1). This band arises mainly from the C═O stretching vibration with minor contributions of the C—N stretching vibration, and the N—H in-plane bend.[31] The latter is responsible for the sensitivity of the amide I band to NH/ND exchanges in the protein backbone. The band shape of the amide I mode can be considered as overlapping bands representing α-helices, β-sheets, turns, and random structures. It is worth noting that there is no vibrational contribution of D_2O to the spectrum of the protein in the amide I region, while the Raman spectrum of H_2O is characterized by a broad band around 1630 cm^{-1} corresponding to the bending vibration of the molecule. To clearly assign the contribution from the different structures to the band shape of the amide I mode, the spectrum of BLG dissolved in D_2O was compared to those of BSA and CHYM

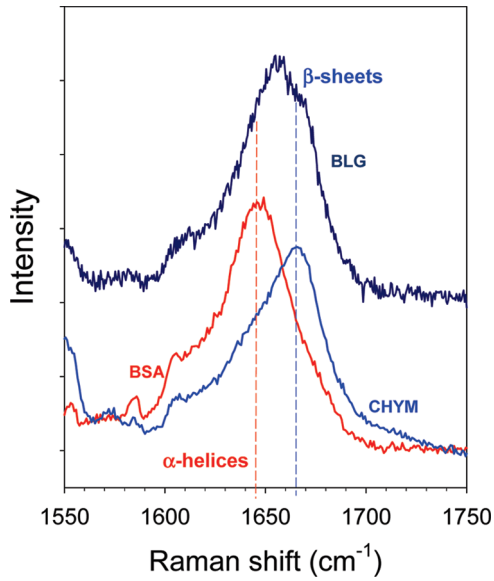

Figure 2. Raman band shape of the amide I mode for BSA, CHYM, and BLG dissolved in D_2O (10 wt %).

in Figure 2. The maximum intensity of the amide I band of BSA, mainly composed of α-helices, indicates the contribution of helical conformation to the spectrum of BLG. The maximum intensity of the spectrum of CHYM, mainly composed of β-sheets,[32] corresponds to the pronounced shoulder observed in the spectrum of BLG, and thus confirms the high β-sheet content in BLG.

The weak intense band around 1550 cm^{-1} is the amide II band (2). It mainly corresponds to a mixture of N−H in-plane bend and C−N stretch. Consequently, this band is also sensitive to the secondary structure and to NH/ND isotopic exchanges. Both amide I and II regions are widely used for secondary structure analysis.[33] However, taking into account its weak intensity in the Raman spectra of the three BLG solutions, the band (2) will not be used to analyze BLG thermal denaturation.

The vibrational composition of the amide III mode is complex, since NH bend contributes to several modes in the 900−1400 cm^{-1} region. However, the range of vibrational frequencies observed for various secondary structures is greater than that for amide I and amide II. The Raman band located around 1240 cm^{-1} (3b) was assigned to β-sheet structure.[21,24,34] It appears as a shoulder of the bending band of D_2O in the 5% BLG solution, and it is distinctively observed for higher concentrations, since β-sheet is the dominant conformation in BLG. The Raman band around 980 cm^{-1} (3′b) has the same origin after N-deuteration. These bands are observed well separated from the amide III mode corresponding to α-helix structures,[21,34] located around 1320 cm^{-1} (3a), and from other bands at 940 and 960 cm^{-1} (4) also associated with α-helical conformation.[21,26,34]

The temperature dependence of the Raman spectrum in the 800−1800 cm^{-1} region was analyzed for monitoring protein denaturation. This region has been decomposed into the amide III band region and the amide I band region to give a clear and detailed description of structural changes. The Raman spectra in both spectral regions are plotted in Figures 3, at room temperature, 65, and 95 °C, marking the temperatures of a two-step process.

First, between 25 and 65 °C (T_{H1}), the spectrum of the amide III region plotted in Figure 3a reveals isotopic exchanges detected from the intensity decrease of the band (3b) at 1240

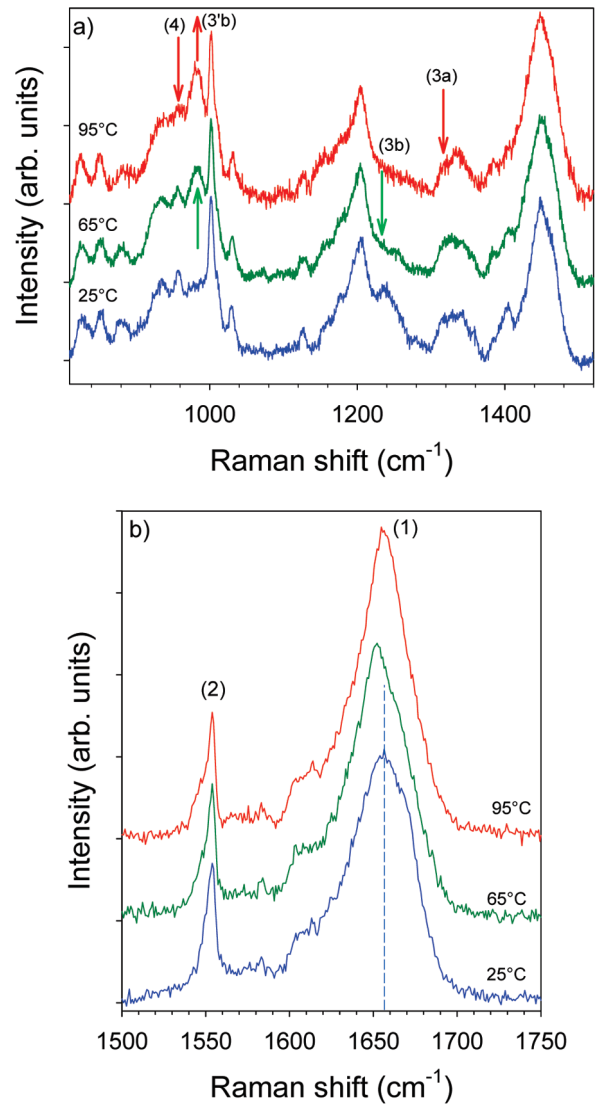

Figure 3. Temperature dependence of the Raman spectra (a) in the amide III region and (b) in the amide I region. Down and up arrows indicate intensity decrease and intensity increase of Raman bands in the amide III region.

cm^{-1} and the concomitant increase of the band (3′b) around 980 cm^{-1}. These additional isotopic exchanges induce a down frequency shift of the amide I band observed in Figure 3b.

Second, between 65 and 95 °C (T_{H2}), the intensity of the Raman band (3′b) is observed to increase with further temperature increase, while almost no change is observed around the position of the Raman band (3b). The intensities of the Raman bands (4) assigned to α-helices are observed to decrease, while the amide I band shifts toward the high frequencies and its band shape becomes symmetric.

To obtain more detailed information from the amide I region, spectrum differences are performed between 65 °C and room temperature and between 95 and 65 °C. Both spectrum differences are reported in Figure 4.

The spectrum difference obtained in the first step of the thermal denaturation between 65 °C and room temperature confirms that the down frequency shift of the amide I band corresponds to isotopic exchanges, since a decrease of intensity around 1670 cm^{-1} is balanced by the increase of intensity around 1650 cm^{-1}. The intensity decrease around 1670 cm^{-1} indicates that isotopic exchanges concern β-sheet structures, according to the observation of the similar balance between intensities of

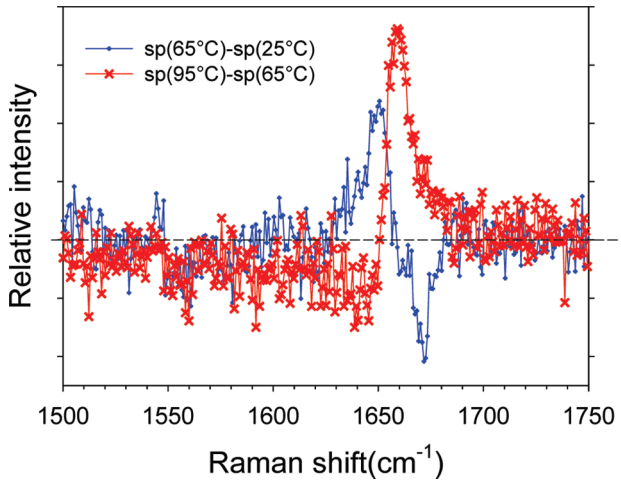

Figure 4. Spectrum differences between 65 °C and room temperature and between 95 and 65 °C.

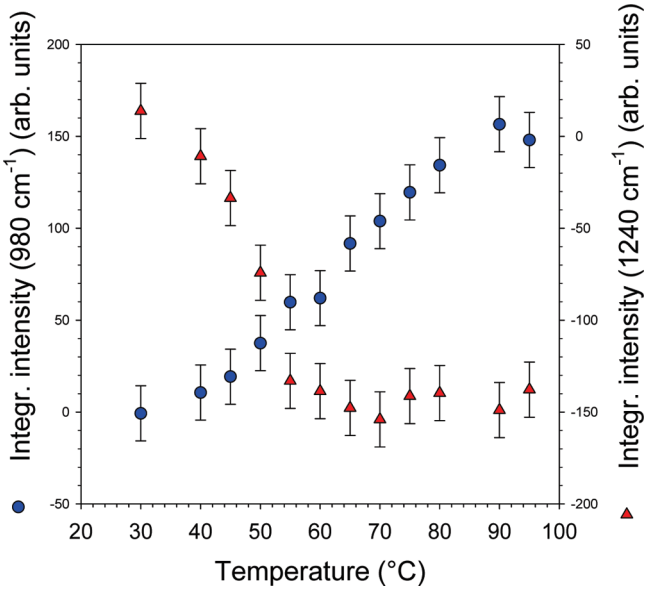

Figure 5. Integrated intensities of Raman amide III (triangles) and III′ (circles) obtained after spectrum differences between T and room temperature.

amide III bands (3′b) and (3b) assigned to β-sheets plotted in Figure 5. These isotopic exchanges could result from the combination of two different phenomena. (i) The first origin could be the dissociation of dimers accompanied with the transformation into R conformation,[30] characterized by the exposition of only one carboxyl group to the solvent. In this context, the strong intensity decrease of the amide III band (3b) at 65 °C cannot only be explained by the N to R transition. (ii) The second origin of the isotopic exchanges is connected to the exposition of the buried hydrophilic residues to the solvent, i.e., the penetration of the solvent into the protein interior allowed by an increased flexibility of the tertiary structure (molten globule state[27]), observed in other globular proteins.[13,16]

The second step of thermal denaturation can be analyzed from the spectrum difference between 95 and 65 °C. The main feature is an increase of intensity around 1660 cm^{-1}, i.e., in the region of the β-sheet structure. This feature is in good agreement with the observation in Figure 5 of a monotonically increasing intensity of the amide III′ band (3′b) from room temperature up to 95 °C, with no concomitant intensity decrease of the amide III band (3b) above 65 °C. Consequently, this feature does not

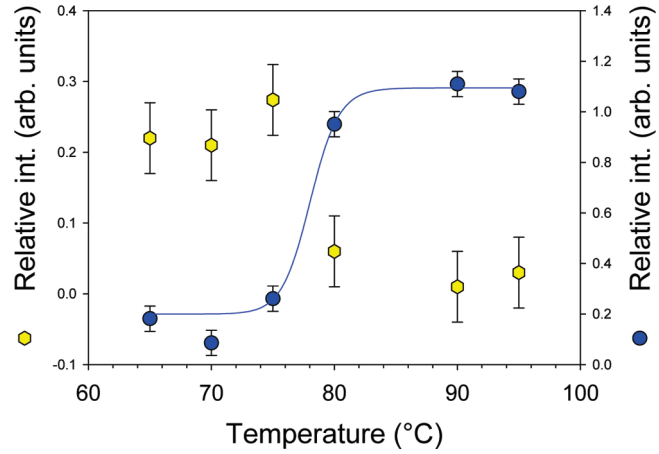

Figure 6. Denaturation curves corresponding to the integrated intensities plotted in Figure 4 around 1640 cm^{-1} (hexagons) associated with the loss of α-helix structure and around 1660 cm^{-1} (circles) associated with the β-sheet formation.

correspond to isotopic exchanges but probably to the signature of the formation of β-sheet structures. A very subtle decrease of the intensity in the spectrum difference can be detected near 1640 cm^{-1}, in the domain of the α-helix structure of the amide I band, which is probably hidden by the overlapping increase of intensity around 1660 cm^{-1}. This decrease is in agreement with the decrease of intensity of Raman bands (4) around 940 and 960 cm^{-1}, and (3′a) around 1320 cm^{-1} observed in Figure 3a, corresponding to α-helix structures. Therefore, the second step could be described as the transformation of α-helical structures into β-sheet structures.

The temperature dependence of the relative intensity around 1650 and 1660 cm^{-1} is plotted in Figure 6. Fitting the temperature dependence of the intensity around 1660 cm^{-1} with a sigmoid leads to the determination of $T_m = 78 \pm 0.7$ °C corresponding to the second stage of the thermal denaturation.

III.1.b. Analysis of the Low-Frequency Raman (LFRS) Spectrum. The scattered low-frequency intensity is transformed into Raman susceptibility ($\chi''(\nu)$) using a procedure detailed in previous studies.[13,14] The Raman susceptibilities of BLG solutions are reported in Figure 7 for different protein concentrations. The spectra of BLG solutions are composed of two broad bands which can be identified from the relevant comparison to the spectra of D_2O and dry BLG plotted in the same figure. The Raman susceptibility is usually considered as roughly representative of the vibrational density of states in molecular disordered systems.[35,36] The high frequency band (II) observed around 170 cm^{-1} in both spectra of D_2O and BLG solutions is assigned to the intermolecular O−D stretching vibrations reflecting the tetrahedral order in water.[37] The analysis of this band in BLG solutions can be used to probe the dynamics of the H-bond network of water. The low-frequency band (I) in BLG solutions can be primarily assigned to the protein dynamics widely influenced by the dynamics of water. The low-frequency band in the LFRS of water (D_2O) is assigned to the cage effect corresponding to the vibrations of a water molecule restricted by neighboring molecules.[38,39]

It is observed that the addition of BLG in water induces a frequency shift toward high frequencies of this band, reflecting a more rigid cage in the presence of BLG, imposed by protein−solvent hydrogen bonding. Consequently, the analysis of this band gives information on the protein dynamics and on the coupling between the protein and solvent dynamics. An intensity decrease of the high-frequency band (II) is clearly

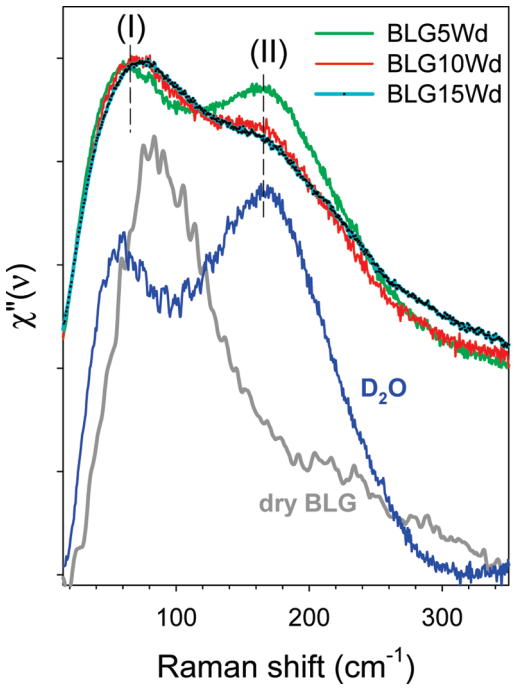

Figure 7. $\chi''(\nu)$ spectra of dry BLG, D_2O, and BLG dissolved in D_2O with 5, 10, and 15 wt % protein concentration.

observed with the increase of protein concentration, reflecting the breakdown of the tetrahedral H-bond network of water.

The temperature dependence of the χ'' spectrum of BLG dissolved in D_2O (with 10 wt % protein concentration) is plotted in Figure 8a. The most important change in the LFRS is related to the band (II) and then reflects significant changes in the hydrogen bond network of water. Slight changes can be detected in the shape of the low-frequency band (I): (i) the broadening of the band (I) observed between room temperature and 60 °C; (ii) the enhancement of the susceptibility in the low-frequency range, near 30 cm^{-1}, is observed in the denatured state at 80 °C (see the arrow and the inset in Figure 8a). The first observation (i) can only be detected from a fitting procedure of all χ'' spectra, using a log-normal function for the band (I) and a Gaussian shape for the intermolecular O−D stretching band (II). The results of this fitting procedure are plotted in Figure 8b at room temperature and $T_{H1} = 60$ °C. Figure 8b clearly shows that (i) there is no enhancement of the intensity in the low-frequency range below 60 °C, (ii) the intensity of the band (II) decreases with temperature, (iii) and the band (I) significantly broadens because of the enhancement of the intensity on the high-frequency side of the band. This enhancement can be related to new strong protein−solvent interactions between hydrophilic side chains of the proteins and water inherent to the dissociation of dimers. In contrast, the detection of enhanced intensity on the low-frequency side of the band (I) observed above 60 °C is related to softer protein−solvent interactions in the protein interior, and probably also to softer water−water interactions at high temperature. A fit of all χ'' spectra gives the temperature dependences of the frequencies of both Raman bands and the intensity of the stretching band (II), reported in Figure 9. This figure reveals an unusual temperature dependence of the frequency of the band (I), since it reflects a strengthening of intermolecular interactions by heating. However, this behavior is probably connected to the enhancement of the intensity on the high-frequency side of the band observed in Figure 8b, and interpreted as the result of the dissociation of dimers. Consequently, the positive ($d\nu/dT$) slope could be the signature of

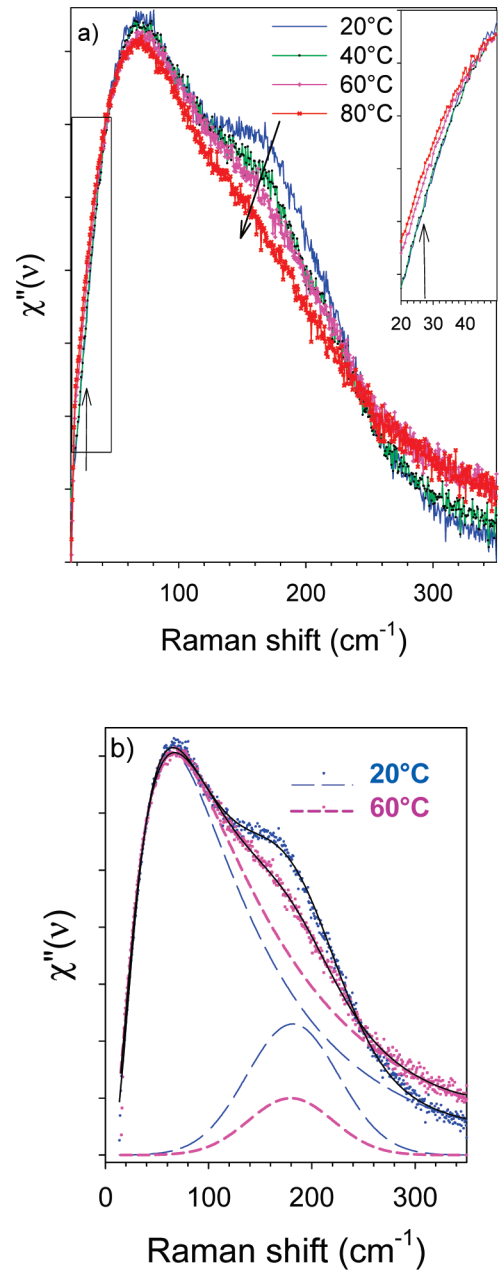

Figure 8. Temperature dependence of the $\chi''(\nu)$ spectrum of BLG dissolved in D_2O (10 wt % protein concentration): (a) From room temperature (native state) up to 80 °C (denatured state). The arrows indicate spectral changes: enhancement of $\chi''(\nu)$ on the low-frequency side of the band (I), clearly observed in the inset, and the softening and the breakdown of the tetrahedral hydrogen bond network of water. (b) Description of the fitting procedure in the native state at room temperature and in the predenatured state at $T_{H1} = 60$ °C. Dashed lines represent the fitted bands corresponding to a log-normal shape for the band (I) and a Gaussian shape for the band (II).

the dissociation of the dimers, observed between the room temperature and 60 °C. Above 65 °C, a down shift of the frequency is clearly observed. It could be the consequence of the enhancement of the intensity on the low-frequency side of the band (I), previously observed for lysozyme[14] and albumin[16] thermal denaturation, and associated with the penetration of the solvent in the protein interior. It is worth noting that both phenomena corresponding to the dimer dissociation and the solvent penetration could overlap on a temperature range which cannot be determined in these experiments.

The most important change directly observed in the χ'' spectrum in Figure 8 by heating corresponds to modifications

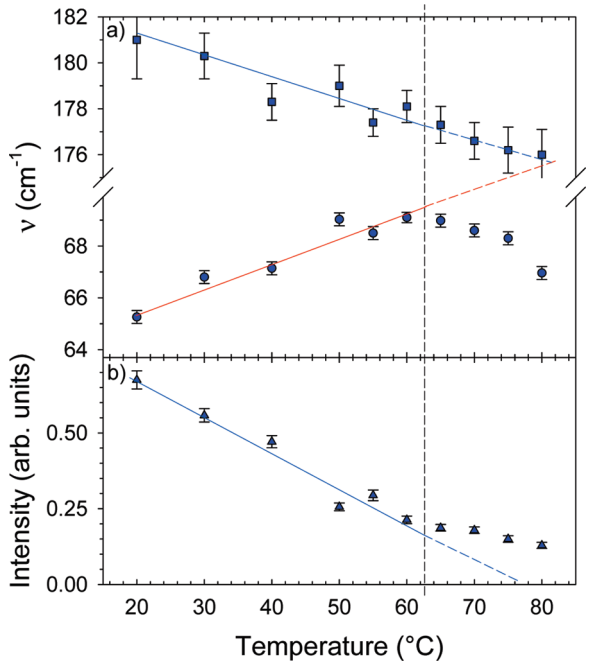

Figure 9. Temperature dependence of the fitted parameters of $\chi''(\nu)$ spectra: (a) frequencies of Raman bands (I) and (II); (b) integrated intensity of the band (II). The full lines correspond to linear regressions of the data between room temperature and 65 °C. The dashed lines correspond to the extension of the linear regressions above 65 °C to point out the deviation of the data in the high temperature range from the linear regression.

in the band shape of intermolecular O−D stretching vibrations. Figure 9 indicates that these changes are related to the intensity decrease and the slight frequency downshift of the band (II). These observations can be interpreted as the breakdown and the softening of the tetrahedral hydrogen bond network of water.[40] A change in the slope of the intensity decrease of the band (II) is clearly observed around 65 °C in Figure 9b. A change in the temperature behavior of the frequency of the band (I) is also observed around 65 °C in Figure 9a. This indicates that the transformation of the tetrahedral hydrogen bond network of water is closely connected to the protein dynamics and also to the protein denaturation process, since the breakdown of the hydrogen bond network between room temperature and 65 °C makes the increase of the protein flexibility more likely, and then favors the dissociation of dimers and the water penetration in the protein interior, both phenomena being associated with isotopic exchanges detected in the amide region in the same temperature range.

III.2. Mechanism of BLG Thermostabilization by Trehalose. ***III.2.a. Influence of Trehalose on the Temperature Dependence of Amide Modes.*** The addition of trehalose induces drastic changes in the amide III region, through the presence of intense broad bands of trehalose in the 800−1400 cm^{-1} spectral range in Figure 10, which overlap with the 1004 cm^{-1} band used for the renormalization of Raman spectra. Consequently, the Raman spectra of BLG solutions containing trehalose were normalized to a Raman band of trehalose located around 1100 cm^{-1} and then cannot be directly compared to Raman spectra of BLG solutions without trehalose.

(i) For the first step of denaturation, isotopic exchanges are determined as described previously without trehalose, from the addition of the integrated intensity of both peaks plotted in Figure 4 from room temperature up to T_{H1}, and normalized for comparison between BLG solutions without trehalose and with

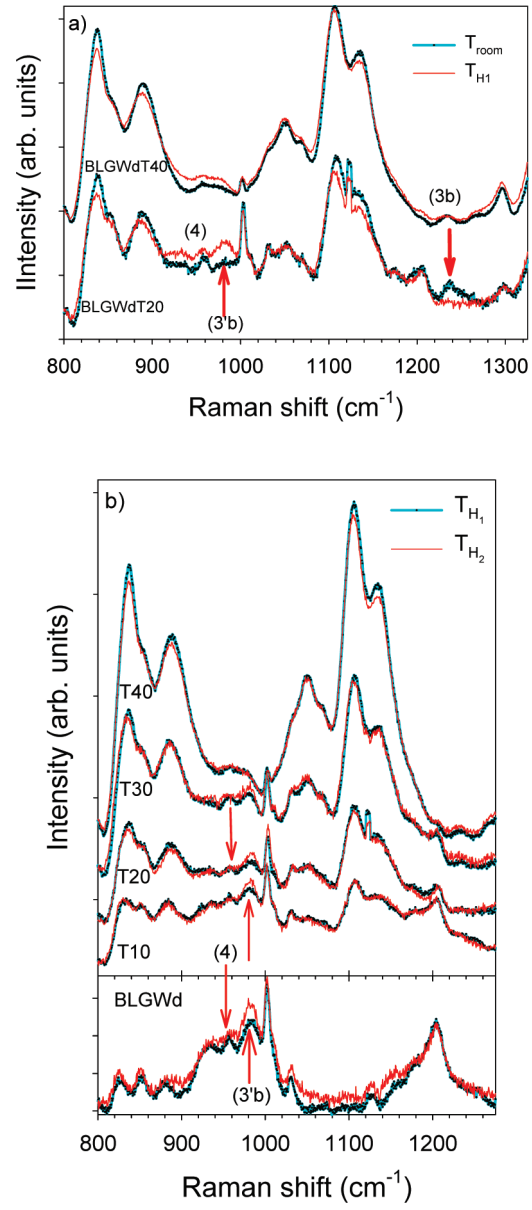

Figure 10. Raman spectra in the amide III region in the presence of trehalose: (a) In the first stage of thermal denaturation between room temperature and T_{H1} for 20 and 40 wt % trehalose. The arrows indicate intensity changes corresponding to isotopic exchanges. (b) In the second stage of thermal denaturation for 0 (BLGWd), 10, 20, 30, and 40 wt % trehalose. The arrows indicate intensity changes corresponding to modifications of the secondary structure; the decrease of intensity at 960 cm^{-1} corresponds to the loss of α-structures, and the concomitant increase at 980 cm^{-1} corresponds to the formation of β-sheets. These changes become imperceptible for trehalose concentrations higher than 20 wt %.

different trehalose concentrations (10, 20, 30, and 40 wt %). The plot of isotopic exchanges in Figure 11a gives denaturation curves for the first step of denaturation. A fit of these curves using a sigmoidal function gives the temperature T_{m1} for the first step of denaturation which is reported in Table 1 for various trehalose concentrations. It is clearly seen that the temperature of the first transformation increases with the trehalose concentration. A maximum of stabilization seems to be reached for 30% trehalose.

Taking into account the difficulty to normalize the Raman spectra from the intensity of the same band for all BLG solutions, it is not possible to give a quantitative comparison

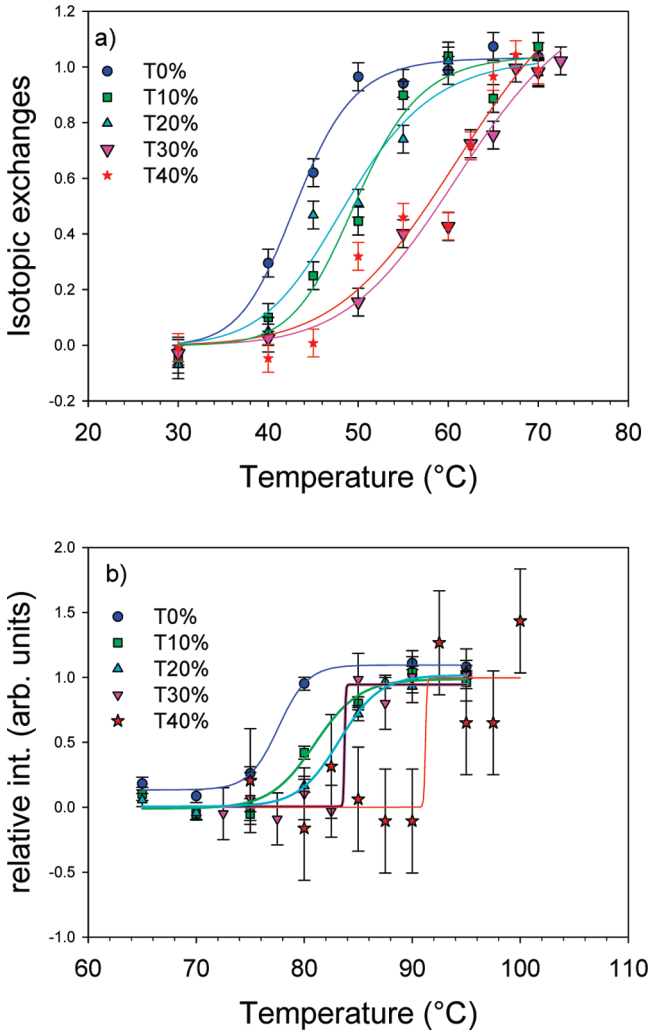

Figure 11. Plot of the denaturation curves, obtained by the sum of the integrated intensity of both peaks reported in Figure 4 for different weighted trehalose concentrations (0, 10, 20, 30, and 40%), corresponding (a) to the first step of denaturation (isotopic exchanges) and (b) to the second step of denaturation (transformation of the secondary structure). The lines correspond to fitted curves using a sigmoidal shape.

TABLE 1: Midpoint Temperatures for BLG Solutions in the Absence and in the Presence of Trehalose, Obtained from a Fitting Procedure of Denaturation Curves Reported in Figure 11, Corresponding to the Two-Step Denaturation Process

	0 wt %	10 wt %	20 wt %	30 wt %	40 wt %
T_{m1} (°C)	43.2 ± 0.7	49.8 ± 1	48.9 ± 2	62.1 ± 3	62.6 ± 5
T_{m2} (°C)	78.0 ± 0.7	81 ± 1	83.2 ± 0.5	83.7 ± 2	91.2 ± 2

between the magnitudes of the isotopic exchanges in the different solutions. However, a qualitative comparison can be provided from the inspection of the spectrum in the amide III and III′ regions. The Raman spectra in this region are plotted in Figure 10a for BLG/W_d/T solutions with 20 and 40 wt % trehalose. It can be observed that the change of the intensity of the Raman bands (3b) and (3′b) between T_{room} and T_{H1} decreases with addition of trehalose. It means that trehalose reduces the exposition to the solvent of the hydrophilic side chains, preserving the dimer association, and probably also limits the accessibility to the solvent of the buried residues in the protein interior.

(ii) The analysis of the influence of trehalose on the second step of thermal denaturation was performed from the calculation of the integrated intensity of the spectrum difference between T ($>T_{H1}$) and T_{H1} in the spectral range 1650−1700 cm^{-1}, plotted in Figure 4 in BLG solutions without trehalose, and previously associated with the formation of β-sheet structure. The plot of this integrated intensity against temperature for BLG solutions in the absence and presence of trehalose is reported in Figure 11b. This figure reveals that addition of trehalose induced a shift of the second step of denaturation toward higher temperatures, as previously observed for the first step of denaturation. Above 20% trehalose, the intensity variations at frequencies assigned to α-helices (intensity decrease around 1645 cm^{-1}) and β-sheets (intensity increase around 1665 cm^{-1}) become very weak, leading to large error bars and change in the shape of the fitting curve. Indeed, the sigmoidal shape of the transformation observed for trehalose concentration lower than 30% becomes sudden and discontinuous for 30 and 40% trehalose. The spectrum of the amide III region plotted in Figure 10b for various trehalose concentrations confirms that the structural changes become very weak with addition of trehalose, and quasi undetectable for 40 wt % trehalose. The amide III band region shows a strong increase of the intensity of the band corresponding to the β-sheets (3′b) and a significant decrease of the intensity of the bands corresponding to α-helices (4), in BLG solutions without trehalose. In the presence of trehalose (<30 wt %), the changes of intensity of these bands are less important, very weak for 30 wt % trehalose, and unobservable for 40 wt % trehalose, in agreement with the very weak changes observed in the amide I band region for concentrations higher than 20 wt %.

Consequently, addition of trehalose results in a shift of the temperature of thermal denaturation, and a limitation of the degree of denaturation, for concentrations higher than 20 wt %, probably induced by a limitation of isotopic exchanges, i.e., a reduction of the accessibility of buried residues to the solvent.

III.2.b. Influence of Trehalose on the LFRS. Addition of trehalose on the LFRS of BLG solutions is analyzed from the plot of χ'' spectra reported in Figure 12 for trehalose concentrations ranging between 0 and 40 wt %. At room temperature, Figure 12a, the main action of trehalose is observed in the spectral range corresponding to the intermolecular O−D stretching vibrations in water (band (II)), thus reflecting modifications in the hydrogen bond water structure. The modification of the band shape results from two effects: (i) the intensity decrease around 170 cm^{-1} and (ii) the concomitant emergence of an additional intensity near 210 cm^{-1}. The first observation (i) reflects that water molecules partially lose the tetrahedral ordering, while the concomitant intensity increase (ii) at higher frequencies (210 cm^{-1}) indicates stronger intermolecular O−D interactions in water, via the formation of new hydrogen bonds between trehalose and water. This is the evidence of the destructuring effect on the tetrahedral water[41,42] leading to the formation of a stiffened hydrogen bond network in water. The concomitant intensity changes at 170 and 210 cm^{-1} increase with addition of trehalose, and the band (II) clearly splits into two components from 30 wt % trehalose, reflecting two organizations of water molecules in the bulk (170 cm^{-1}) and in hydration shells of trehalose (210 cm^{-1}) in line with previous studies on different sugars.[43−45] Contrary to the O−D stretching band (II), addition of trehalose does not change the shape of the low-frequency band (I) at room temperature. This indicates that the protein dynamics is similar in the absence and presence of trehalose, and no trehalose−protein interaction can be

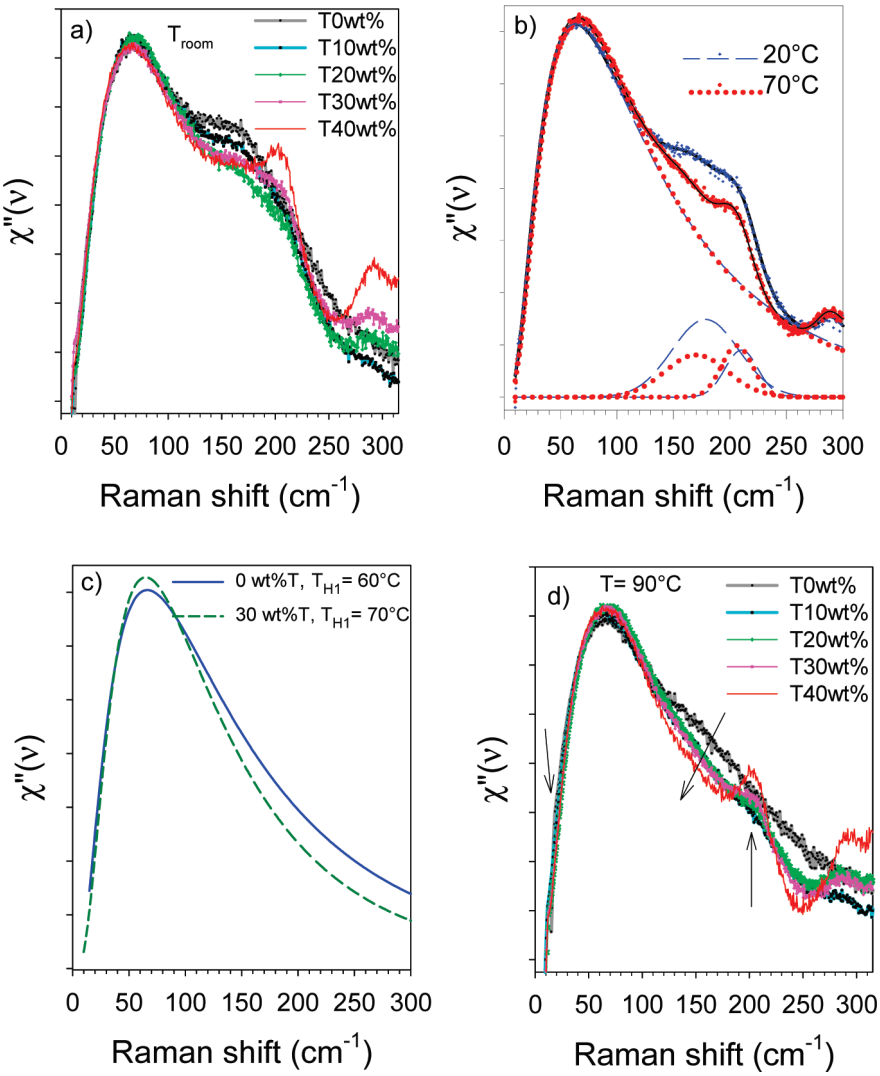

Figure 12. Raman susceptibility of BLG solutions for various trehalose concentrations: (a) in the native state at room temperature; (b) description of the fitting procedure in the native (room temperature) and predenatured (T_{H1} = 70 °C) states for 30 wt % trehalose; (c) comparison of the fitted low-frequency band (I) in the absence and in the presence of 30 wt % trehalose; (d) in the denatured state at 90 °C.

detected in agreement with the hypothesis predicting the preferential exclusion of disaccharides around the protein surface.[1,12]

The fitting procedure of $\chi''(\nu)$ spectra is shown in Figure 12b for 30 wt % trehalose at room temperature and at T_{H1} = 70 °C, to analyze the transformation of the $\chi''(\nu)$ spectrum in the presence of trehalose in the first step of denaturation. This figure reveals that the enhancement of the susceptibility on the high frequency side of band (I) is limited in the presence of trehalose compared to Figure 8b in the absence of trehalose. A second piece of information concerns the decrease of the intensity of the low-frequency component of the band (II) reflecting the loss of the tetrahedral organization of water molecules, previously observed in the absence of trehalose in Figure 8b. It is observed that the second component (210 cm^{-1}) of the band (II) remains nearly temperature independent between the room temperature and T_{H1}. The log-normal function used in the fitting procedure is plotted in Figure 12c for BLG solutions without trehalose and with 30% trehalose at temperatures corresponding to T_{H1}. It is observed that the band (I) is significantly sharper in the presence of trehalose, because of a lower contribution of the enhanced susceptibility on the high-frequency side of the band (I). This observation should correspond to a weaker dissociation of dimers in the presence of trehalose.

The χ'' spectra are also plotted in Figure 12d in the fully denatured state to point out the influence of trehalose on the thermal denaturation process. This plot reveals that spectral modifications induced by addition of trehalose are observed in the whole LFRS (10−300 cm^{-1}) of the denatured state and located by three arrows. In the low-frequency range (~30 cm^{-1}), the enhanced intensity detected by heating is observed to decrease with addition of trehalose at temperatures above T_{H1}, related to a reduction of the degree of denaturation in the presence of trehalose. The analysis of the band (II) clearly shows that the component around 210 cm^{-1} remains observable in the denatured state even for low trehalose concentrations, whereas a decrease of intensity near 170 cm^{-1} is clearly detected. This result indicates that addition of trehalose stabilizes the distorted hydrogen bond network of water and then maintain the protein dynamics, which appears very similar at room temperature and at 90 °C for BLG solutions with 40 wt % trehalose. The temperature dependence of the frequency of this band is plotted in Figure 13 for several trehalose concentrations. The frequencies are determined from the fitting procedure depicted in Figure 12b. It is worth noting that, for trehalose concentrations higher than 20 wt %, two Gaussian peaks are needed to fit the shape of the band (II) in the $\chi''(\nu)$ spectra. At 20 wt % trehalose, the unusual shift toward high frequencies of the band (II) observed

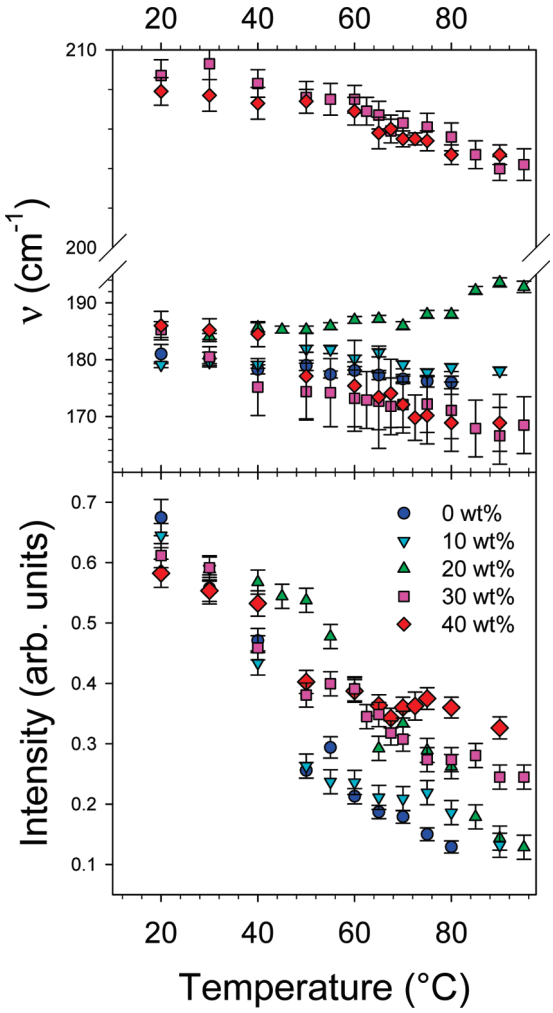

Figure 13. Temperature dependence of fitted parameters of the intermolecular O−D stretching band (II) in $\chi''(\nu)$ spectra, in the absence and presence of trehalose: (a) $\nu(T)$ plot, corresponding to the temperature dependence of the frequency; (b) $I(T)$ plot, corresponding to the temperature dependence of the integrated intensity of the band (II). For trehalose concentrations higher than 20 wt %, two Gaussian functions are used to obtain a satisfactory agreement between the experimental shape of the band (II) and the calculated $\chi''(\nu)$ spectra. In this case, the fitted integrated intensity corresponds to the sum of the intensity of both components.

for the high temperatures is induced by the intensity decrease of the 170 cm^{-1} component, i.e., the loss of the tetrahedral structure of water, while the intensity of the component corresponding to the distorted hydrogen bond network does not change. The integrated intensity of the band (II) for 30 and 40 wt % trehalose was obtained by summation of the intensity of both components at 170 and 210 cm^{-1}. A clear reduction of the intensity decrease is observed for these trehalose concentrations, in the high temperature range ($T > 60$ °C). Consequently, 30 wt % appears as a threshold concentration for the distortion of the hydrogen bond network of water and then for the stabilization of the organization of water molecules, in line to the study of the BLG thermostabilization by trehalose in the amide band region.

IV. Concluding Remarks

The mechanism of BLG thermal denaturation (for BLG (10 wt %) dissolved in D_2O at pD 6.9) can be carefully detailed from Raman investigations carried out simultaneously in the 800−1800 cm^{-1} region of the amide bands and in the 10−350 cm^{-1} low-frequency range. In the temperature range from room temperature up to 100 °C, BLG denaturation can be described as a two-step process. It is worth noting that additional structural changes could occur above 100 °C, as suggested in several works.[46,47] The first step corresponds to the dissociation of dimers associated with an increase of flexibility of the tertiary structure, and then can be interpreted as the transformation of the native state into the so-called "molten globule" state. In the second step of the denaturation, conformational changes are detected and described as a loss of α-helix structures and a concomitant formation of β-sheets.

The low-frequency analysis indicates that the softening and the breakdown of the hydrogen bond network are responsible for the dissociation of dimers and then the penetration of D_2O in the monomer, leading to the destabilization of the secondary structure. The investigation of the low-frequency Raman susceptibility gives the unique opportunity to detect the dissociation of the dimers through the analysis of the low-frequency and predominant band (I) in the $\chi''(\nu)$ spectrum, reflecting the protein dynamics and the coupling of the protein and solvent dynamics. The enhancement of the intensity on the high-frequency side of the band (I), assigned to strong interactions between D_2O and polar side chains of the protein, leads to a shift of the band (I) toward the high frequencies. No direct signature of the dimer dissociation has been evidenced at higher frequencies, in the spectral range corresponding to the molecular fingerprint of the protein. The examination of Figure 9 indicates that the dimer dissociation occurs progressively, as the transformation of the hydrogen bond network, by heating from room temperature up to 60 °C.

At higher temperatures ($T = 80$ °C), the transformation of the tertiary structure in a more flexible structure and the loss of α-helix structures favor additional protein−D_2O interactions within the tertiary structure. The consequence is the enhancement of $\chi''(\nu)$ intensity on the low-frequency side of the band (I), reflecting the detection of new soft interactions between the solvent and the core of the protein, mainly composed of hydrophobic residues. Consequently, investigations in the low-frequency $\chi''(\nu)$ spectrum give information on the dynamics of the solvent, via the analysis of the band (II), which controls the motions of the protein through the coupling of the protein and the solvent dynamics, probed from the analysis of the shape of the band (I).

The analysis of amide modes gives direct information on molecular conformational changes in the secondary structure, and also indirect information on the tertiary structure through the observation of isotopic exchanges between the protein and the solvent. By heating BLG solutions from room temperature up to 60 °C, only isotopic exchanges are detected through spectral modifications in the amide I and III regions. These changes have been assigned to the dissociation of dimers and to the penetration of the solvent in the protein interior, only possible in a highly flexible tertiary structure. By monitoring these amide modes, modifications of the secondary structure are detected with further heating of BLG solutions above T_{H1}. The spectral changes observed near 960 and 1320 cm^{-1} in Figure 3a and near 1645 cm^{-1} in Figure 4 clearly reflect the loss of α-structures, while a concomitant formation of β-sheets is detected through the intensity increase of the Raman bands corresponding to amide mode III′ (980 cm^{-1}) and amide mode I (1660 cm^{-1}).

The main effect of trehalose on BLG solutions primarily corresponds to modifications in the shape of the intermolecular O−D stretching band (II) in the $\chi''(\nu)$ spectrum, reflecting a transformation of the tetrahedral structure of water into a stiffened network. No significant change in the shape of the low-frequency band (I) is detected, in line with the hypothesis predicting the

preferential exclusion of trehalose from the protein surface.[1,12] Trehalose stabilizes the quaternary structure and also makes the tertiary structure more rigid and then more stable upon heating, in agreement with other investigations.[48] A threshold concentration of 30 wt % was determined for the action of trehalose on the properties of the hydrogen bond network of water, which is related to the mechanism of BLG thermostabilization. Below 30%, the presence of trehalose induces a mere shift of the denaturation curves toward high temperatures, while, in the presence of 30% trehalose, partial thermal denaturation is observed in Figure 10b. At the highest concentration (40 wt %), isotopic exchanges are very weak (see Figure 10a, where the intensity of the 1240 cm^{-1} band remains nearly constant) and no spectral change can be detected in Figure 10b, which suggests no conformational change of BLG. However, the careful analysis of the amide I band reveals a very slight transformation of the secondary structure, as reported in Figure 11b. Consequently, a hierarchical stabilization of the protein structures is observed for the highest trehalose concentration. The native secondary structure is quasi preserved, because the solvent penetration in the protein interior is limited by the stabilization of the tertiary and quaternary structures, which arises from the stabilization of the distorted hydrogen bond network of water.

BLG is characterized by a secondary structure mainly composed of β-sheets and the existence of a quaternary structure corresponding to dimer associations. The present work can be compared to the results obtained on other proteins characterized by different molecular weights and structural properties. Similar investigations have been carried out on lysozyme[14] (14.3 kDa), composed of α-helix structures (41%) and β-sheets (21%), and bovine serum albumin[16] (66 kDa), mainly composed of α-helices (51%). The main effect of trehalose on protein solutions, commonly observed for these proteins, is the transformation of the tetrahedral organization of water into a stiffened hydrogen bond network. The consequence is the stabilization of the distorted hydrogen bond network of water and then the stabilization of the most important structural edifice of the protein, i.e., the tertiary structure for lysozyme and albumin and the quaternary structure for β-lactoglobulin. Another common feature observed in these analyses is the reduction of the exposition of protein residues to the solvent in the presence of trehalose. However, this observation concerns different kinds of residues depending on the structural properties of the protein. For lysozyme characterized by a low molecular weight, trehalose is only preventing the solvent accessibility of buried residues in the tertiary structure during heating above 60 °C, while in albumin (characterized by a high molecular weight) a reduction of the exposition of hydrophilic side-chain residues around the protein surface is detected at room temperature. For β-lactoglobulin, trehalose preserves the dimer association upon heating and then limits the exposition of side-chain residues on the surface of monomers, and also limits the accessibility of the buried residues in the tertiary structure to the solvent, upon further heating.

These common features induced by trehalose on different kinds of proteins dissolved in water are probably connected to the ability of trehalose to distort the tetrahedral structure of water and then to its exceptional capabilities to form hydrogen bonds with water, previously analyzed in recent works.[17,42,49]

Acknowledgment. This work was supported by the ANR (Agence Nationale de la Recherche) through the BIOSTAB project ("Physique Chimie du Vivant" program), by FEDER and by Nord-Pas de Calais region.

References and Notes

(1) Xie, G.; Timasheff, S. N. *Biophys. Chem.* **1997**, *64*, 25.
(2) Kaushik, J. K.; Bhat, R. *J. Biol. Chem.* **2003**, *278*, 26458.
(3) Carpenter, J. F.; Prestrelski, S. J.; Arakawa, T. *Arch. Biochem. Biophys.* **1993**, *303*, 456.
(4) Prestrelski, S. J.; Arakawa, T.; Carpenter, J. F. *Arch. Biochem. Biophys.* **1993**, *303*, 465.
(5) Arakawa, T.; Prestrelski, S. J.; Kenney, W. C.; Carpenter, J. F. *Adv. Drug Delivery Rev.* **2001**, *46*, 307.
(6) Green, J. L.; Angell, C. A. *J. Phys. Chem.* **1989**, *93*, 2880.
(7) Timasheff, S. N. *Biochemistry* **2002**, *41*, 13473.
(8) Belton, P. S.; Gil, A. M. *Biopolymers* **1994**, *34*, 957.
(9) Magazu, S.; Branca, C.; Faraone, A.; Migliardo, F.; Migliardo, P.; Romeo, G. *Physica B* **2001**, *301*, 126.
(10) Crowe, L. M.; Reid, D. S.; Crowe, J. H. *Biophys. J.* **1996**, *71*, 2087.
(11) Leslie, S. B.; Israeli, E.; Lighthart, B.; Crowe, J. H.; Crowe, L. M. *Appl. Environ. Microbiol.* **1995**, *61*, 3592.
(12) Arakawa, T.; Timasheff, S. N. *Biochemistry* **1982**, *21*, 6536.
(13) Hédoux, A.; Ionov, R.; Willart, J. F.; Lerbret, A.; Affouard, F.; Guinet, Y.; Descamps, M.; Prevost, D.; Paccou, L.; Danède, F. *J. Chem. Phys.* **2006**, *124*, 14703.
(14) Hédoux, A.; Willart, J. F.; Ionov, R.; Affouard, F.; Guinet, Y.; Paccou, L.; Lerbret, A.; Descamps, M. *J. Phys. Chem. B* **2006**, *110*, 22886.
(15) Hedoux, A.; Affouard, F.; Descamps, M.; Guinet, Y.; Paccou, L. *J. Phys.: Condens. Matter* **2007**, *19*, 8 p.
(16) Hedoux, A.; Willart, J. F.; Paccou, L.; Guinet, Y.; Affouard, F.; Lerbret, A.; Descamps, M. *J. Phys. Chem. B* **2009**, *113*, 6119.
(17) Lerbret, A.; Bordat, P.; Affouard, F.; Hedoux, A.; Guinet, Y.; Descamps, M. *J. Phys. Chem. B* **2007**, *111*, 9410.
(18) Branca, C.; Magazu, S.; Migliardo, F.; Migliardo, P. *Physica A* **2002**, *304*, 314.
(19) Anderle, G.; Mendelsohn, R. *Biophys. J.* **1987**, *52*, 69.
(20) Cai, S.; Singh, B. R. *Biophys. Chem.* **1999**, *80*, 7.
(21) Ngarize, S.; Herman, H.; Adams, A.; Howell, N. *J. Agric. Food Chem.* **2004**, *52*, 6470.
(22) D'Alfonso, L.; Collini, M.; Baldini, G. *Biochemistry* **2002**, *41*, 326.
(23) Lapanje, S.; Poklar, N. *Biophys. Chem.* **1989**, *34*, 155.
(24) Ikeda, S.; Li-Chan, E. *Food Hydrocolloids* **2004**, *18*, 489.
(25) Qi, X. L.; Brownlow, S.; Holt, C.; Sellers, P. *Biochem. Soc. Trans.* **1995**, *23*, 74S.
(26) Nonaka, M.; Li-Chan, E.; Nakai, S. *J. Agric. Food Chem.* **1993**, *41*, 1176.
(27) Qi, X. L.; Holt, C.; McNulty, D.; Clarke, D. T.; Brownlow, S.; Jones, G. R. *Biochem. J.* **1997**, *324*, 341.
(28) Qi, X. L.; Brownlow, S.; Holt, C.; Sellers, P. *Biochim. Biophys. Acta* **1995**, *1248*, 43.
(29) Blanch, E. W.; Hecht, L.; Barron, L. D. *Protein Sci.* **1999**, *8*, 1362.
(30) Tanford, C.; De, P. K. *J. Biol. Chem.* **1961**, *236*, 1711.
(31) Surewicz, W. K.; Mantsch, H. H.; Chapman, D. *Biochemistry* **1993**, *32*, 389.
(32) Williams, R. W.; Dunker, A. K. *J. Mol. Biol.* **1981**, *152*, 783.
(33) Dousseau, F.; Pezolet, M. *Biochemistry* **1990**, *29*, 8771.
(34) Young, M. J.; B, C.-M.; Ozaki, Y. *J. Phys. Chem. B* **2000**, *104*, 7812.
(35) Hedoux, A.; Derollez, P.; Guinet, Y.; Dianoux, A. J.; Descamps, M. *Phys. Rev. B* **2001**, *63*, 144202/1.
(36) Achibat, T.; Boukenter, A.; Duval, E. *J. Chem. Phys.* **1993**, *99*, 2046.
(37) Walrafen, G. E.; Chu, Y. C.; Piermarini, G. J. *J. Phys. Chem.* **1996**, *100*, 10363.
(38) Nakayama, T. *Phys. Rev. Lett.* **1998**, *80*, 1244.
(39) Padro, J. A.; Marti, J. *J. Chem. Phys.* **2003**, *118*, 452.
(40) Walrafen, G. E.; Fisher, M. R.; Hokmabadi, M. S.; Yang, W. H. *J. Chem. Phys.* **1986**, *85*, 6970.
(41) Branca, C.; Magazu, S.; Maisano, G.; Migliardo, P. *J. Chem. Phys.* **1999**, *111*, 281.
(42) Lerbret, A.; Bordat, P.; Affouard, F.; Guinet, Y.; Hedoux, A.; Paccou, L.; Prevost, D.; Descamps, M. *Carbohydr. Res.* **2005**, *340*, 881.
(43) Affouard, F.; Bordat, P.; Descamps, M.; Lerbret, A.; Magazu, S.; Migliardo, F.; Ramirez-Cuesta, A. J.; Telling, M. T. F. *Chem. Phys.* **2005**, *317*, 258.
(44) Perticaroli, S.; Sassi, P.; Morresi, A.; Paolantoni, M. *J. Raman Spectrosc.* **2008**, *39*, 227.
(45) Paolantoni, M.; Sassi, P.; Morresi, A.; Santini, S. *J. Chem. Phys.* **2007**, *127*, 24504/1.
(46) Paulsson, M.; Hegg, P.-O.; Castberg, H. B. *Thermochim. Acta* **1985**, *95*, 435.
(47) de Wit, J.; Klarenbeek, G. *J. Dairy Res.* **1981**, *48*, 293.
(48) D'Alfonso, L.; Collini, M.; Baldini, G. *Eur. J. Biochem.* **2003**, *270*, 2497.
(49) Ionov, R.; Hédoux, A.; Guinet, Y.; Bordat, P.; Lerbret, A.; Affouard, F.; Prevost, D.; Descamps, M. *J. Non-Cryst. Solids* **2006**, *352*, 4430.

JP1006022